Synchrotron x-ray scattering studies of water intercalation in a layered synthetic silicate

G. J. da Silva* and J. O. Fossum†
Department of Physics, Norwegian University of Science and Technology, NTNU, N-7491 Trondheim, Norway

E. DiMasi
Physics Department, Brookhaven National Laboratory, Upton, New York 11973-5000

K. J. Måløy
Physics Department, University of Oslo, Oslo, Norway

S. B. Lutnæs
Department of Physics, Norwegian University of Science and Technology, NTNU, NO-7491 Trondheim, Norway
(Received 8 March 2002; published 22 July 2002)

Synchrotron x-ray diffraction studies were performed on a synthetic layered silicate Fluorohectorite clay. Diffraction patterns along the stacking direction were obtained in surface reflection and bulk transmission geometries on bulk pressed samples under controlled temperature and relative humidity. One-dimensional structure factors modeling the positions of the intercalant atoms have been obtained for three stable hydration states. From the narrow $(00l)$ peak widths we conclude that well-crystallized domains consist of stacks of about 100 platelets, forming crystallites of the order of 0.1 μm thick. These crystallites have an orientational angular distribution of about 24° around the stacking direction and represent the solid framework for microporosity in these samples.

DOI: 10.1103/PhysRevE.66.011303 PACS number(s): 81.05.Rm, 61.43.Gt, 71.20.Tx, 78.70.Ck

I. INTRODUCTION

Clays, or layered silicates, have been widely studied and discussed as geological materials, and modern industrial uses of clays are based on this history and knowledge [1,2]. Clays are layered solids, which can be classified into three groups according to the rigidity of the layers with respect to distortions involving atomic displacement transverse to the layer plane [3]. This classification divides the layered solids into three classes. Class I describes layered solids that are composed of monatomic thin planes of atoms and can easily sustain long-wavelength deformations transverse to the layer planes. Examples include graphite and boron nitride. Class II materials are typically composed of three distinct planes of strongly bonded atoms and are more resistant to transverse distortions than the previous class. Some such materials are layer dichalcogenides and metal chlorides. Clays are class III materials, where the layers can be quite thick. They are the stiffest of lamellar solids, and quite rigid against transverse layer distortions. Most of the natural clays are very heterogeneous mixtures of minerals, and this can cause both experimental and theoretical difficulties. However, pure clays can now be made synthetically. Here the well-controlled chemistry and structure enable detailed experimental investigation, including recent advances in atomic scale measurements made by synchrotron and other modern techniques [4]. A powerful complement for the experimentalists comes from simulation methods, due to the development of fast computers and efficient algorithms. In some cases simulations suggest new experiments, which suggest further simulations. The present work represents an experimental step in this direction. Clays have the unique ability to be pillared by intercalated guest ions (Fig. 1), making their study of fundamental importance within the general context of ''nanosandwiches'' as a basis for nanotechnologies [5]. For this reason there is also a trend to include clays into modern materials science [6] together with other and sometimes better understood synthetic and complex adaptive materials such as colloids, polymers, liquid crystals, and biomaterials. The small particle size and microporous structure of clays give them their extremely important capability to absorb water. A hydrated clay is a complex system. The detailed interactions between the interlayer cation, coordinating water molecules, and charged silicate surface lead to static structural properties and hydration dynamics that are still not well understood. A better theoretical description of hydrated clays is important for technology. For example, the type of intercalated cation in this kind of system may be exchanged, and this also enables manufacturing of so-called pillared layered structures (PLS's) in which large cations are intercalated. These cations serve as spacers between face-to-face or edge-to-face connected clay sheets. These dry nanoporous systems may be used industrially as molecular sieves, or as catalysts with large accessible surface areas. The PLS's have been and may still be utilized by physicists as model systems to study transport in a well-characterized customized nanoporous medium [7].

In this paper we report the results of *in situ* x-ray diffraction experiments performed on the synthetic Smectite clay Na-Fluorohectorite at the National Synchrotron Light Source

*On leave from Institute of Physics, University of Brasília, CP 04513, 70919-970, Brasília-DF, Brazil. Electronic address: geraldo.silva@phys.ntnu.no
†Electronic address: jon.fossum@phys.ntnu.no

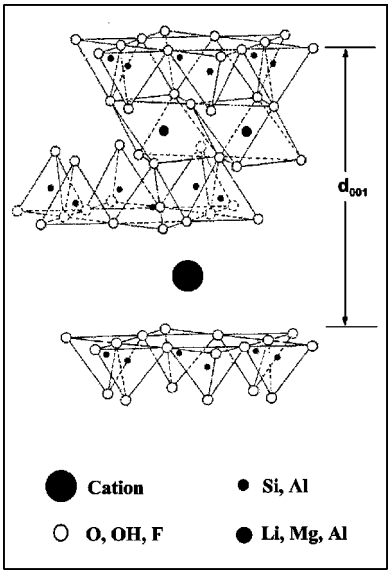

FIG. 1. The structure of a typical 2:1 layered silicate clay. On the right the basal spacing d_{001} is indicated and below are the symbols for some typical elements of clay components.

at Brookhaven National Laboratory. Na-Fluorohectorite has the chemical formula per half unit cell Na_x-$(Mg_{3-x}Li_x)Si_4O_{10}F_2$. Hectorite is a 2:1 phyllosilicate, meaning that the platelets are formed by two inverted silicate tetrahedral sheets, sharing their apical oxygens with one octahedral sheet sandwiched in between (see Fig. 7 below). It is classified as a trioctahedral smectite since Li^+ substitutes for Mg^{2+} in the octahedral sheet sites, which are fully occupied. Fluorohectorites differ from natural hectorites in that the OH groups have been replaced by F. The proportion x of the Li^+ ions determines the surface charge of the platelets, which are held together in the stacked structure by an interlayer cation: in our case, $x=0.6$ Na^+ ions per half unit cell. Among the smectites, polydisperse Fluorohectorite has one of the largest values for particle diameter, up to more than 10 μm [8]. Water can be intercalated in between each platelet causing the clay to swell. For Na-Fluorohectorite this intercalation process, which can be controlled by temperature and relative humidity, yields three stable hydration states. The structures, referred to as having either 0, 1, or 2 intercalated water layers, are quite well ordered along the stacking direction. The unit cell along the stacking direction is given by the distance between the stacked platelets, and is around 1.0 nm for the case of 0 water layers and 1.2 and 1.5 nm for the cases of one and two water layers, respectively. The main objectives of the present study are to determine the structural properties of this material, such as the particle morphology, amount of intercalated water, and relationship between the intercalant structure and clay layers. Details of the experimental conditions and sample preparation are given in Sec. II. In Sec. III we present the results and analysis, and some concluding remarks are presented in Sec. IV.

II. DESCRIPTION OF EXPERIMENTS

Fluorohectorite was purchased in powder form from Corning, Inc. Our pressed samples of Na-Fluorohectorite were prepared [9] by dissolving and stirring clay powder in distilled water and adding an amount of sodium ions corresponding to about 10 times the known surface charge per unit cell. The result was a two-phase solution, one clear-water phase at the top and one white-water clay phase at the bottom. After taking out the clear phase and repeating this process at least twice, the resultant solution was left to dialyze for a period of one month. Every second day the distilled water was replaced, and the old dialyzed water was tested for excess Cl^- ions using a standard silver nitrate procedure. Dried samples of Na-Fluorohectorite were obtained using a load cell specially designed for this purpose [9]. Initially at room temperature a load of 500 N was applied to the sample, providing a pressure of 120 kPa. In a further step the temperature was raised to 72°C maintaining the load. In order to remove as much water as possible from the sample the load was removed and the temperature raised to 110°C. The final dried samples had a density of 1.8 g/cm^3 and thickness around 0.5 cm appropriate for the synchrotron x-ray diffraction studies.

The x-ray scattering measurements were conducted at beamline X22A at the National Synchrotron Light Source, using an x-ray wavelength of $\lambda=0.1196$ nm, a four-circle diffractometer with a vertical scattering plane, and a focused beam spot about 0.4 mm high and 1 mm wide. Slits before the NaI scintillator detector, 0.5 or 1.0 mm high and 2 mm wide, mainly determined the instrumental resolution. This was estimated from measurements of the (111) and (004) reflections of a silicon single crystal placed at the sample position. The approximately Gaussian widths of these peaks showed a linear dependence on the momentum transfer q($q \equiv 4\pi \sin\theta/\lambda$), which was extrapolated to the q positions of the clay Bragg peaks for the analysis.

The x-ray studies were conducted under controlled temperature and humidity. To control the humidity, air was pumped through either a saturated saltwater solution [10] or a silica gel desiccant column, and circulated through a sample chamber consisting of a beryllium metal can closed by vacuum tight flanges. Inside this chamber the sample was glued to a copper block having an embedded heating element, and mounted on a thermoelectric Peltier cooling element. Close to the sample, the temperature was measured using a copper-Constantan thermocouple mounted inside the copper block. The temperature was raised and lowered in 5°C or greater steps in the range 0 to 130°C, at relative humidity levels near either 100% or 0%, to determine the conditions that stabilize each of the three hydration states.

Two scattering geometries were used in these studies (see Fig. 2). In Fig. 2(a) we show a schematic representation of the reflection geometry utilized for the analysis of the surface of the sample. It will be referred to as the *surface scattering geometry*. In Fig. 2(b) we show the *bulk scattering geometry* for diffraction in transmission through the sample interior. In this case, a foil of lead was placed on the sample surface facing the x-ray beam in order to prevent any kind of surface contribution to the bulk studies. We differentiate betweensurface and bulk due to our preliminary experimental results pointing to very different transient time constants linked to

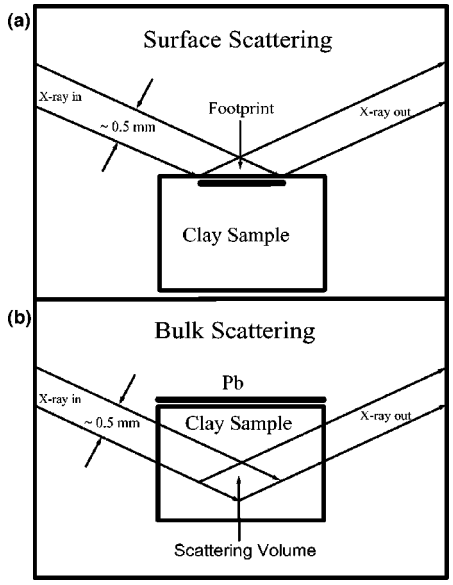

FIG. 2. Schematic representation of the experimental arrangement utilized for the analysis of the surface scattering geometry (a) and of the bulk scattering geometry (b) of the sample.

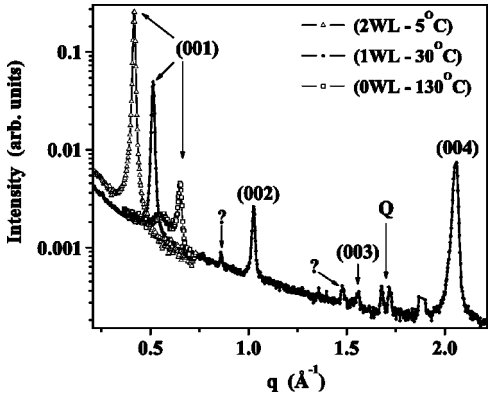

FIG. 3. Bulk scattering geometry diffraction pattern. For one water layer (1WL) the peaks 001–004 are present. The symbols *Q* and ''?'' refer to quartz and some unidentified mineral impurities. For 0WL and 2WL only the (001) peaks are shown. The legend shows typical values of the temperature.

the process of water absorption and deabsorption in the cooling and heating processes for these two cases [11].

III. EXPERIMENTAL RESULTS AND DATA ANALYSIS

A representative one-dimensional diffraction pattern is shown in Fig. 3, for the case of bulk scattering geometry at different temperatures. For one water layer (1WL) several orders of (00l) peaks are present, along with a collection of sharper peaks which can be attributed to quartz (labeled *Q* in Fig. 3) and other unidentified mineral impurities (labeled with ?). For the dehydrated (0WL) and further hydrated (2WL) cases, we show the intensity near the (001) peaks. We observed that during hydration scattered intensity appears between the commensurate Bragg peak positions, and this is a well-known signature of disordered intercalation or mixed intercalation along the stacking direction. For example, in the case of 0WL the small ''satellite'' peak (exaggerated by the logarithmic scale) near the 1WL peak position shows a coexistence of these two regimes of hydration. In such mixed regimes the Hendricks-Teller [12] formalism applies, as we will discuss in future reports that describe this hydration-dependent scattering in detail [13]. For the stable hydration states in the present study, the (00*l*) peak positions can be described as multiples of a single *d* spacing for each hydration state, as shown in Table I.

The (00*l*) peaks are broadened beyond the instrumental resolution. To obtain the deconvoluted peak widths intrinsic to the sample, we fitted to the pseudo-Voigt peak shape function often used for synchrotron data [14]. For our purpose this function provides a good approximation to the convolution of Lorentzian and Gaussian functions [15]:

TABLE I. Fitted peak positions values shown in Figs. 4(a) and 4(b). The mean distances between the planes for the cases of zero, one, and two water layers and for the surface and bulk scattering geometries are also shown.

	Surface scattering geometry		Bulk scattering geometry	
	q_c (Å^{-1})	d_{mean} (Å)	q_c (Å^{-1})	d_{mean} (Å)
0WL	001→0.643	9.69±0.06	001→0.650	
	002→1.297		002→1.301	
	003→1.952		003→1.968	9.63±0.04
	005→3.257		005→3.265	
1WL	001→0.504	12.38±0.07	001→0.513	
	002→1.014		002→1.026	
	004→2.037		004→2.060	12.24±0.02
	006→3.060		006→3.078	
2WL	001→0.411	15.17±0.08	001→0.416	
	002→0.828		003→1.248	
	003→1.246		005→2.079	15.107±0.004
	007→2.913		007→2.911	

$$\Phi(q)=\frac{2\eta}{\pi\Gamma(1+4(q-q_c)^2)}+2\frac{1-\eta}{\Gamma}\left(\frac{\ln 2}{\pi}\right)^{1/2}e^{-4\ln 2(q-q_c)^2/\Gamma^2}. \quad (1)$$

Φ is related to the measured intensity by $I(q)=C(q)\Phi(q)$. The C parameter is related to scattering structure and polarization factors, as we discuss further below, and can be approximated by a constant value in the region around each (00l) peak since it varies slowly with q compared to the peak widths. For the region of the (001) peaks where these factors fall steeply, a linear in q dependence corresponding to the fits in Fig. 4 was added to the background in the peak fitting procedure. Γ is the experimental width at the half maximum of the curves and η is a mixing constant that ranges from zero to one, and is responsible for changing the shape of the resulting curve from Gaussian to Lorentzian. The widths of the Gaussian and Lorentzian components, denoted by Ω_G and Ω_L, respectively, are related to Γ and η by [16]

$$\Gamma=(\Omega_G^5+2.6927\Omega_G^4\Omega_L+2.4284\Omega_G^3\Omega_L^2+4.471\Omega_G^2\Omega_L^3+0.0784\Omega_G\Omega_L^4+\Omega_L^5)^{1/5}, \quad (2a)$$

$$\eta=1.36603\frac{\Omega_L}{\Gamma}-0.47719\frac{\Omega_L^2}{\Gamma^2}+0.11116\frac{\Omega_L^3}{\Gamma^3}. \quad (2b)$$

The linewidth of the Gaussian component is generally attributed to the instrumental resolution [17]. Hence, we assign Ω_G from the linear interpolation

$$\Omega_G=4.83\times10^{-3}\ \text{Å}^{-1}-0.449\times10^{-3}q \quad (3)$$

obtained from measurements of Si single-crystal Bragg peaks. As an example of the Gaussian contribution, see Figs. 4(a) and 4(b) for the peaks 002. Utilizing Eq. (3) for Ω_G, we fitted the peak shapes of Figs. 4(a) and 4(b) to Eq. (1). For both surface and bulk scattering geometry and for the cases of 0WL, 1WL, and 2WL, we obtained the Ω_L values. The result is plotted in Fig. 5. For these Lorentzian components, the broadening of the curves can be considered mainly to be due to the size or thickness of crystallized domains, which we take to equal the entire thickness of a particle, and their lattice strain or disorder in the lattice spacing (interpreted as $\xi=\Delta d/d$), which lends a q dependence to the width. Our studies of Na-Fluorohectorite particles in colloidal suspension provide evidence to support our interpretation of the domain thickness as equivalent to the particle thickness [11]. The size and strain related broadening may be determined by graphing the experimental data in the form of a Williamson-Hall [18] style plot according to the following relations, written in terms of the wave vector q:

$$\Omega_L=\frac{2\pi}{Nd}+\xi q. \quad (4)$$

The slope of the straight line gives the strain ξ, and the intercept at $\Omega_L=0$ estimates the mean clay particle thickness (Nd). In Fig. 5(a) (surface scattering geometry) and Fig. 5(b) (bulk scattering geometry) we show the plots for the widths Ω_L versus peak positions q for the three cases, fitted with Eq. (4). Independent of the hydration state, the mean value for N is around 100, showing that the sample is composed of crystallites with thickness of about 0.1 μm. The strain ξ is of the same order for the samples but varies slightly between the two scattering geometries, 0.5% for the bulk and 0.2% for the surface. We obtained the same value of 0.5% from a powder diffraction measurement of a separate Na-Fluorohectorite sample in the 1WL hydration state [19]. Figures 4(a) and 4(b) for the peaks 002 show that the widths Ω_L are similar to the widths Ω_G.

The measured intensity $I(q)$ depends on the scattering structure factor $G(q)$, the Lorentz-polarization factors $L_p(q)$, represented above as $C(q)$, and the interference function $\Phi(q)$. $I(q)$ is thus given by [20]

$$I(q)\propto|G(q)|^2L_p(q)\Phi(q). \quad (5)$$

In our analysis, Φ is given by the pseudo-Voigt form discussed above, and so it remains to model the q dependence of the remaining factors, along with a geometric angle-dependent correction for the illuminated sample region, illustrated in Fig. 2. Considering the Fluorohectorite compound as a centrosymmetric system, it permits us to write the structure factor as

$$G(q)=2\sum_j n_jf_je^{-W_jq^2/(4\pi)^2}\cos(qZ_j). \quad (6)$$

The summation is taken over all the atoms of the unit cell and n_j refers to the number of atoms of the type j located a distance Z_j from the plane of the Mg and Li atoms, which has been selected as the origin of the structure. W_j are the Debye-Waller temperature correction factors. For the intercalants we consider the atomic scattering factor f_j of the constituents and we use a single Debye-Waller factor $W_j=W=1.6$ [20]. For the Lorentz-polarization factors the generally known expression [21] ($L_p=2P/\sin 2\theta\sin\theta^\nu$) is

$$L_p=\frac{P}{\sqrt{1-\zeta^2q^2}(\zeta q)^{\nu+1}}, \quad (7)$$

where $\zeta=\lambda/4\pi$ and P is the polarization contribution, which depends on the x-ray source. At the synchrotron the x rays are linearly polarized in the horizontal plane. In our case the scattering was in the vertical plane and for this case P = 1 [22]. The exponent ν is related to the number of crystals favorably oriented for diffracted intensity to be accepted into the detector at a given Bragg angle. In the limit of a high resolution measurement, $\nu=0$ for a perfect crystal and $\nu=1$ for a perfect powder [22]. For natural clays and for finite resolution measurements, the correct ν value is unknown, and at most one can say that it is between these two cases [21]. The results of our fits of the peak intensities versus peak positions are shown in Fig. 6 for the two sample geometries and the three hydration states. The positions Z_j and the proportions of each element of the intralayer clay sheet were

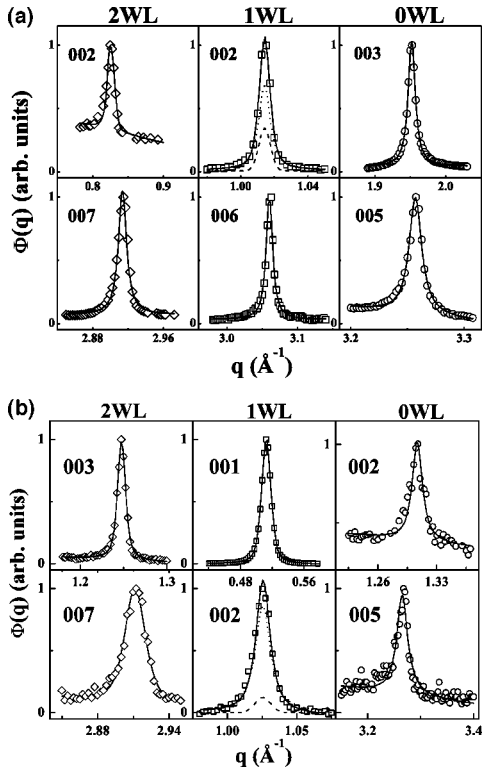

FIG. 4. Selected peaks for the line shape analysis of the (a) surface scattering geometry and (b) bulk scattering geometry. Each column of figures represents one of the WL regimes. The symbols are the experimental data and the continuous line the fitted result to Eqs. (1) and (2) plus linear background. The dashed and the dotted lines on the peak 002 for the 1WL regime show the Gaussian and Lorentzian contributions, respectively.

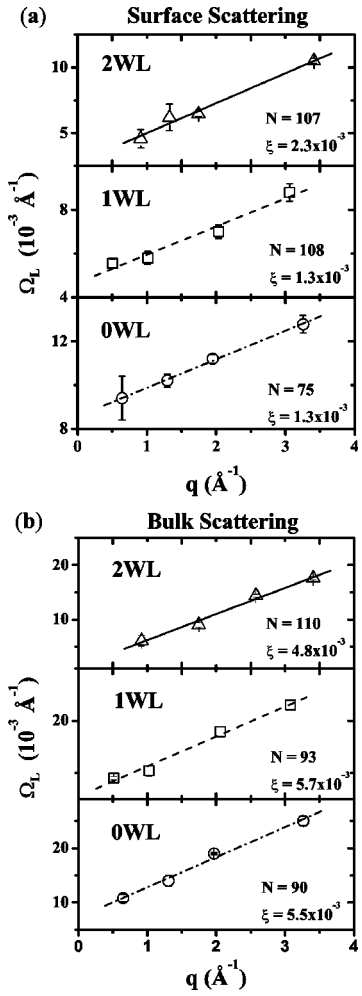

FIG. 5. Williamson-Hall plot for the (a) surface scattering geometry and (b) bulk scattering geometry. The triangle, square, and circle symbols are the Lorentzian widths obtained from the fitting procedure using Eqs. (1) and (2). The straight lines were fitted to Eq. (4) and their values are presented in each figure for the cases of 0WL, 1WL, and 2WL. Also in each figure the number N of stacked platelets and the value of the strain ν are given.

obtained from the literature [8,23], and maintained constant during the fitting procedure. Under some restrictions, the fitted parameters were the exponent ν, and the proportions of the water molecules intercalated between the platelets. See Sec. IV for details.

In Fig. 7 we show a schematic representation for the Z_j positions and for proportions of each element comprising a half top of a silicate layer plus half of the space between two platelets. On the same figure we present the model structures for the one and two water layer cases. The figure is divided into two regions, taking as the origin the center of symmetry of the platelet, meaning the positions of the Li and Mg atoms. The upper half shows the positions (labeled on the left side) and the proportions (right side) for the elements of the 1WL case. For example, the value 6.16 Å is the half distance between platelets for this case. The lower region shows the positions and the proportions of the elements for the 2WL case. Table II summarizes the fitted and nonfitted values shown in Fig. 7. The fitted ν value was obtained by consid-

TABLE II. Values of proportions n and positions Z(Å) of the elements comprising the Na-Fluorohectorite unit cell for the cases of zero, one, and two water layers.

Silicate layer		Zero water layers		One water layer		Two water layers	
n	Z(Å)	n	Z (Å)	n	Z(Å)	n	Z (Å)
0.6Li+2.4Mg	0.0	0.6Na	4.83	0.6Na	5.67	0.40Na	5.65
2F+4O	1.09			(1.2±0.2)H_2O	6.16	0.20Na	7.52
4Si	2.70					(2.8±0.2)H_2O	6.41
6O	3.28						

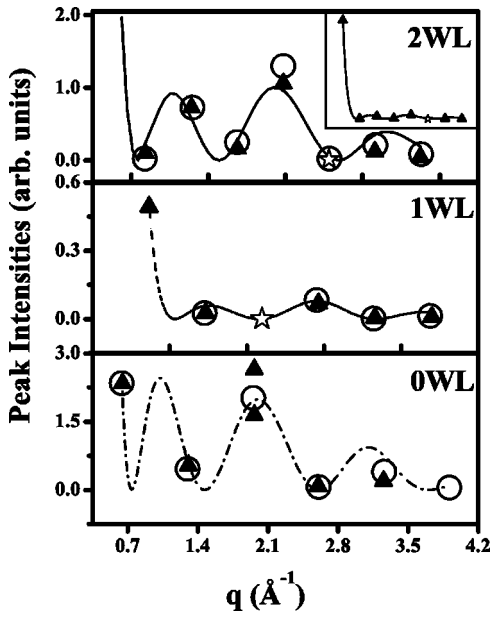

FIG. 6. Peak intensities as a function of peak positions for the cases of 0WL, 1WL, and 2WL. The open circles represent the surface reflection experimental data and the closed triangles represent the bulk transmission experimental data. The lines were fitted to $|G|^2 L_p$, for the 2WL and 1WL bulk transmission data, and for 0WL surface data. Star symbols indicate bulk transmission peaks that were absent within our statistics.

ering the 0WL and 1WL case. For the 0WL case it is reasonable to assume that the Na cation is situated at the half distance between platelets and the obtained n value is $\nu = 0.94 \pm 0.16$. For the 1WL case $\nu = 0.98 \pm 0.14$. This represents a measure of the orientational angular distribution of crystallites about the stacking direction, as obtained from rocking curves of peak intensity as a function of the sample orientation angle θ. The rocking curve shown in Fig. 8, for a surface (003) peak at $T = 80°\mathrm{C}$ and relative humidity of 75%, is typical for our samples. It shows that at half maximum, the crystallites have an angular distribution of about 12° with respect to the vertical stacking axis.

IV. DISCUSSION

In order to get the results of our fits of the integrated Bragg peak intensities we need to make some assumptions. In our fitting procedure, we have considered as constant the positions and proportions of the atoms of the silicate structure (see Fig. 7). Consequently, due to the electrical balance, the proportion of the Na cations in the interlayer between silicates is assumed constant. For the interlayer, the proportions of the water components were fitted and their positions fixed. The values of the positions for each element in the Z direction perpendicular to the layer planes were taken from density profile analysis of reported numerical simulations of clay systems [24] and scaled to the distance between our clay layers (see Table I). After such considerations, we determined the value of the parameter ν for the 0WL and 1WL cases, as discussed above. For the 2WL case (Fig.7), the positions of the Na cation were divided into two values according to the result of Skipper *et al.* [24]; we assumed a 0WL and 1WL mean value for ν as constant, and we fitted the proportions of the interlayer water components of Table II. Finally, for the atoms of the silicate structure we checked the sensitivity of our results to variations in some fixed parameters. For example, for the Li and Mg atoms we permitted a small deviation from the central position $Z = 0$, by a value of order $+/-0.2$ Å. Also, the positions of H_2O molecules were permitted to vary by the same value and the results were not affected in a significant way.

The results of Table II show that the ratio of the proportion of water molecules to the proportion of Na cations is 2.0 ± 0.2 for the 1WL case, and 4.7 ± 0.2 for the 2WL case. These results are in agreement with those obtained from [24] where the authors found 2.1 and 4.9 water molecules around each Na cation, respectively. Even if the present results seem reasonable compared to those of [24], we must comment on their applicability. The simulated system from where we took the initial values for our fits is a Na-Smectite with chemical formula $Al_4Si_8O_{20}(OH)_2$. The layer charge density and distances between the planes of this system have comparable values to those we find in our experiments. A more detailed analysis is required for comparison, but given the limited q range of our one-dimensional diffraction study, detailed modeling of the silicate structure is not justified here. However, it shows the promising possibility of the interplay between simulation results and experiment, and we are presently in the process of performing a Monte Carlo simulation of the Na-Fluorohectorite. Our preliminary simulation results [25] are in agreement with the present experiments. Also, our preliminary data may show experimental evidence for changes to the clay structure factor during the hydration and dehydration processes, in the form of slight peak shifts and changing proportions of peak intensities. These details will be discussed in forthcoming publications [13]. Such studies may benefit as well from the application of additional, complementary x-ray techniques sensitive to ordering within the basal planes. From the Williamson-Hall analysis, the contribution to the line broadening due to disorder is of the same order of magnitude for the samples but varying slightly between the two scattering geometries, 0.5% for the bulk and 0.2% for the surface. These values can be considered small, but it is worthwhile to compare them. The bulk scattering geometry and powder diffraction are expected to give the same values for the strain because we have made powder samples by grinding a powder from a bulk sample, thus producing individual grains equivalent to small bulk samples [19]. We found the same value for the strain in our powder sample as in our bulk scattering experiment [19]. The different values of strain obtained between the surface and bulk scattering geometries could be explained by easier stress relaxation at the surface. Our samples are composed of well-crystallized particles with thickness of the order of magnitude 0.1 μm or about 100 platelets. This number of platelets remains around the same even in a situation when the crystallites are suspended in a solution, in which case they are in the 2WL limit of hydration [26]. This robust morphology of thick particles, from which the clay cannot exfoliate into thinner silicate sheets, is attributed to the large intrinsic layer

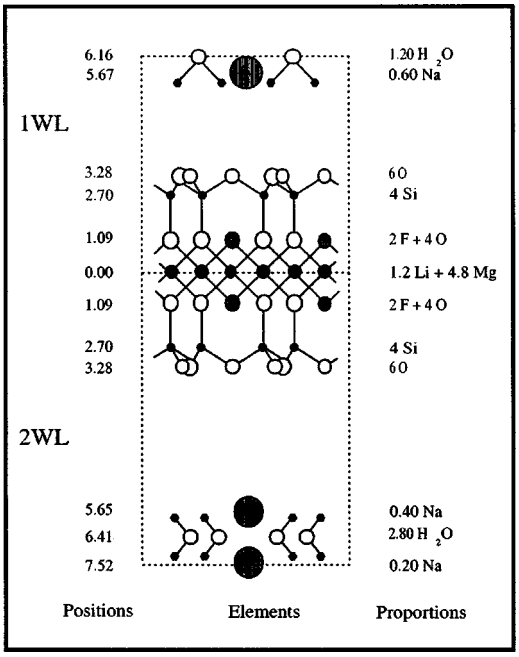

FIG. 7. Schematic representation of the elements comprising the Na-Fluorohectorite unit cell. The origin position (0 Å) was chosen to be the symmetry center of the silicate. The upper region of the figure shows the positions and proportions of the elements for the case of 1WL; the lower portion is the 2WL case. See also Table II.

charge of the Na-Fluorohectorite sample. Our mean value 0.96 ± 0.16 for the exponent ν in Eq. (3), considering the 0WL and 1WL cases, is typical for natural clay minerals [21] with almost the same orientational angular distribution.

V. SUMMARY

In this paper we have shown the results of synchrotron x-ray studies performed on synthetic Na-Fluorohectorite clay. Using the NSLS beamline X22A at Brookhaven National Laboratory, we have studied interlayer Bragg peaks as a function of temperatures between 0 and 130°C, and at relative humidities near 100% and near 0%. Data obtained by scattering from surfaces in reflection and scattering in transmission through the bulk were compared and found to exhibit essentially the same structure and water content, in agreement with Skipper *et al.* [25]. The ratios of intercalated water to cation were obtained. A Williamson-Hall analysis of the peak widths suggests near perfect crystallites of about 0.1 μm thickness and small but significantly different strain values for the two geometries.

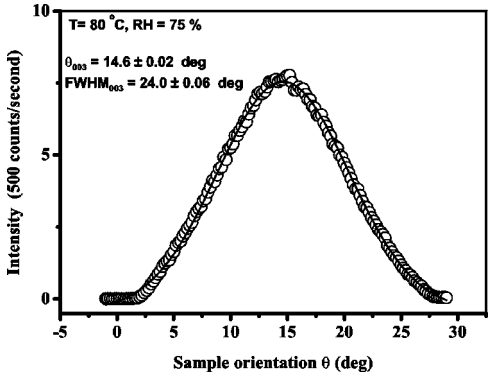

FIG. 8. Rotating anode surface rocking scan around the 003 peak of one Na-Fluorohectorite sample at a temperature T of 80 °C and at 75% relative humidity (RH), fitted to a Gaussian with the (003) peak at $\theta_{003} \approx 14.6°$ and a full width at half maximum $\mathrm{FWHM}_{003} \approx 24°$.

ACKNOWLEDGMENTS

G.J. d. S. acknowledges the Conselho Nacional de Desenvolvimento Científico e Tecnológico (CNPq/Brazil) for financial support. J.O.F. thanks the Norwegian Research Council (NFR) for financial support and also NTNU/NFR Grant No. SUP115185/420 for support during the early part of this work. The National Synchrotron Light Source is supported by the DOE under Contract No. DE-AC02-98CH10886.

[1] R.E. Hummel, *Understanding Materials Science* (Springer-Verlag, New York, 1998).
[2] B. Velde, *Introduction to Clay Minerals* (Chapman and Hall, London, 1992).
[3] S. Lee and S.A. Solin, Phys. Rev. B **43**, 12 012 (1991).
[4] R.T. Cygan, in *Reviews in Mineralogy and Geochemistry*, edited by R. T. Cygan and J. D. Kubicki (Mineralogical Society of America, Washington, D.C., 2001), Vol. 42, Chap. 1, p. 1.
[5] C. Oriakhi, Chem. Br. **34**, 59 (1998).
[6] S.A. Solin, Annu. Rev. Mater. Sci. **27**, 89 (1997).
[7] J.O. Fossum, in *Soft Condensed Matter: Configurations, Dynamics and Functionality*, edited by A.T. Skjeltorp and D. Sherrington (Kluwer Academic, Amsterdam, 2000).
[8] P.D. Karivatna, T.J. Pinnavaia, and P.A. Schroeder, J. Phys. Chem. Solids **57**, 1897 (1996).
[9] S.B. Lutnæs, Diploma thesis, Faculty of Physics, Informatics and Mathematics, Norwegian University of Science and Technology, Trondheim, Norway, 1999.
[10] David R. Lide, in *CRC Handbook of Chemistry and Physics*, edited by H.P.R. Frederikse (CRC Press, Boca Raton, FL, 1997), Vol. 78, p. 15–24.
[11] E. DiMasi, J.O. Fossum, and G.J. da Silva, in *Proceedings of the 12th International Clay Conference* (Elsevier, Amsterdam, in press).
[12] S. Hendricks and E. Teller, J. Chem. Phys. **10**, 147 (1942).
[13] G.J. da Silva *et al.* (unpublished).
[14] L.W. Finger, in *Modern Powder Diffraction*, edited by D.L. Bish and J. E. Prost (Mineralogical Society of America, Washington, D.C., 1989), Vol. 20, p. 309.
[15] G.K. Wertheim, M.A. Butler, K.W. West, and D.N.E. Bucha-

nan, Rev. Sci. Instrum. **45**, 1369 (1974).
[16] D.E. Cox, J.B. Hastings, L.P. Cardoso, and L.W. Finger, Mater. Sci. Forum **9**, 1 (1986).
[17] D.E. Cox, B.H. Toby, and M.M. Eddy, Aust. J. Phys. **41**, 117 (1998).
[18] G.K. Williamson and W.H. Hall, Acta Metall. **1**, 22 (1953).
[19] B. Noheda, E. DiMasi, J.O. Fossum, and G.J. da Silva (unpublished).
[20] G.W. Brandly and G. Brown, *Crystal Structure of Clay Minerals and Their X-ray Identification* (Mineralogical Society, London, 1980), Vol. 5, Chap. 4, p. 257.
[21] Duane Milton Moore and Robert C. Reynolds, Jr., *X-ray Diffraction and the Identification and Analysis of Clay Minerals*, 2nd ed. (Oxford University Press, New York, 1997), Vol. 1, p. 90.
[22] Jens Als-Nielsen and Des McMorrow, *Elements of Modern X-ray Physics* (John Wiley & Sons, Chichester, England, 2001), Vol. 1, Chap. 1, p. 9.
[23] J.R. Walker, in *Computer Application to X-ray Powder Diffraction Analysis of Clay Minerals*, edited by R.C. Reynolds, Jr., and J.R. Walker (Clay Minerals Society, Aurora, CO, 1993), Vol. 5, Chap. 1, p. 1.
[24] N.T. Skipper, K. Refson, and J.D.C. McConnell, J. Chem. Phys. **94**, 7434 (1991).
[25] G.J. da Silva, A. Hansen, and J.O. Fossum (unpublished)
[26] E. DiMasi, J.O. Fossum, T. Gog, and C. Venkataraman, Phys. Rev. E **64**, 061704 (2001).